RSC Advances

PAPER

View Article Online
View Journal | View Issue

Cite this: *RSC Adv.*, 2023, **13**, 2611

A novel hyperbranched polyethyleneimine–graphene composite as shale inhibitor for drilling fluid

Luo Zhao, [ab] Heming Zhu, [a] Guoliang Tian [bc] and Yuxiu An *[b]

One of the principal conundrums in drilling operations is addressing wellbore instability caused by shale hydration. Therefore, it is crucial to develop high-performance shale inhibitors. In this work, a hyperbranched polyethyleneimine/graphene composite (HPEI-G) was prepared by blending at 60 °C, and it was then used as a shale inhibitor. The inhibition performance of HPEI-G was verified using mud making test, linear swelling test and sedimentation test. The mechanism of HPEI-G was researched and determined using Fourier transform infrared spectroscopy (FT-IR), X-ray diffraction (XRD), particle size distribution test and scanning electron microscopy (SEM). The compatibility of HPEI-G with the basic water-based drilling mud (WBM) was also verified. It can be observed from the results of the linear swelling test that 0.5 wt% HPEI-G reduced the swelling rate of montmorillonite (MMT) to 30.36%, and 1 wt% of KCl only decreased the swelling rate of MMT to 43.83%. In addition, HPEI-G is compatible with WBDF. The inhibition mechanism of HPEI-G included chemical adsorption and physical blockage. HPEI-G was adsorbed on the surface and interlayer of MMT by hydrogen bonding and electrostatic attraction, reducing the diffuse electric double layer to inhibit the hydration of MMT. The sheets of graphene in HPEI-G allowed it to stick on the surface of the shale and plug the nanopores of the shale, preventing the access of water. The inhibition effect of HPEI-G over a temperature range from room temperature to 150 °C was considered to be excellent.

Received 1st November 2022
Accepted 23rd December 2022

DOI: 10.1039/d2ra06919a

rsc.li/rsc-advances

1. Introduction

Prevention of wellbore instability caused by shale hydration is one of the principal conundrums in drilling operations,[1–3] because consequences of wellbore instability include the increase in drilling time and expense. The wellbore instability can be caused by mechanical and chemical factors.[4,5] It is the chemical factors caused by the interaction between the shale and the drilling fluid that cause the instability of the wellbore. Controlling of shale swelling is the effective way to solving the instability of the wellbore. Oil-based drilling fluids (OBDFs) with better inhibition, lubricity and high temperature resistance are the best choice.[6] The OBDFs control the instability of the wellbore by clogging the clay nanopores and forming a protective film on the surface of the shale,[7,8] but they are too expensive, and have a significant environmental impact. Water-based drilling fluids (WBDFs) are widely used because of their low cost and environmental friendliness.[9,10] However, the long-term interaction between the WBDFs and shale formations causes shale hydration and swelling, leading to a variety of problems that can occur in the wellbore. Shale inhibitors can inhibit the hydration caused by the interaction of clay minerals with the water of the WBDFs. Therefore, the development of high-performance shale inhibitors is crucial.

There are various inhibitors used in shale formations to control the stability of the wellbore, such as potassium chloride (KCl), amines, polymers and nanomaterials. KCl is the main inorganic salt inhibitor.[11] However, the inhibition impact of KCl is limited. The inhibition ability of amine-based shale inhibitors is better than that of KCl, and amine-based shale inhibitors have been widely studied and applied. The inhibition mechanism of polymer inhibitors is mainly the formation of a dense film.[12] Nanomaterials reduce the contact of water molecules with shale surfaces by sealing micropores,[13] and nano silica (SiO_2) combined with amine compounds can also be used for reservoir acidising alteration.[14,15] But these shale inhibitors are limited by a variety of conditions, including poor heat resistance, limited inhibition ability, environmental issues, complex preparation processes, and high costs. The hyperbranched polyethyleneimine (HPEI) is well-known for its adsorption, solubility, versatility and synergistic stability.[16] There have been

[a]*Key Laboratory of Shale Oil and Gas Enrichment Mechanism and Development, Sinopec Research Institute of Petroleum Engineering, Changping District, Beijing 100101, China. E-mail: zl192400@163.com; zhuhm.sripe@sinopec.com*

[b]*School of Engineering and Technology, China University of Geosciences (Beijing), Haidian District, Beijing 100083, China. E-mail: anyx@cugb.edu.cn; 13522045597@163.com; 634348643@qq.com*

[c]*The Sixth Geological Brigade of Shandong Bureau of Geology and Mineral Resources, Weihai City, Shandong Province, 264209, China*

studies on the introduction of HPEI as a shale inhibitor in WBDF and its inhibition capabilities have been evaluated,[17] but these researches have not been complex enough, thorough or systematic.

Graphene is a widely studied material with unique characteristics. Compared to polymer materials, graphene has higher filtration loss property.[18] The nano-flake structure of graphene enables it to block pores on the surface of the shale and reduces the contact of water with the shale. Compared to inorganic nanomaterials, composites based on graphene and amine compounds caused lower filtration losses after dispersion in drilling fluids, and exhibited better inhibition.[19] The enhanced inhibition property of graphene result in better rheological properties and inhibition of hydration.[20,21] A variety of graphene materials have been developed as shale inhibitors, which have grafted with cetyltrimethylammonium, glucopyranose and polyethyleneimine.[22–24] The inhibition effect of graphene materials was better than that of traditional inhibitors, but the preparation process was complex, and the maximum temperature of the performance tests was only 65.5 °C. Therefore, the thermal stability of graphene composites at higher temperatures needs to be studied. Composites based on the hyperbranched polymer and graphene can show an improvement of the structural stability of clay mineral particles by hyperbranched polymer, in addition to the improvement of rheology and filtration by graphene.

In this study, a hyperbranched polyethyleneimine/graphene composite (HPEI-G) was prepared by thermal polymerisation and used as a shale inhibitor. The inhibition performance of HPEI-G was verified using several inhibition evaluation methods, and the inhibition mechanism was investigated. The compatibility of HPEI-G to WBM was also evaluated.

2. Materials and methods

2.1 Materials

HPEI (molecular weight 10 000, 98 wt%) was purchased from Gongbike Polymer Materials Company, and the graphene paste (GO, high water solubility, 8 wt% solid content) was purchased from Xianfeng Nanomaterials Company. The KCl was purchased from the Aladdin Biochemical Technology Company, and sodium carbonate (Na_2CO_3) was purchased from the Cologne Chemicals Company. Montmorillonite (MMT), xanthan gum (XC), low-viscosity carboxymethyl cellulose sodium (CMC-LV), polyacrylamide (PAM) and barite were supplied by the Xinjiang Oil Field. All the materials were used without further purification.

2.2 Methods

2.2.1 Preparation of HPEI-G. The preparation process is shown in Fig. 1. Firstly, 25 mL of GO was dispersed in 175 mL of deionised water, and then 20 g of HPEI was poured into the liquid to give a mass ratio of 1 : 10. Finally, the mixture was stirred at 60 °C for 8 h to give a black opaque liquid, during which, HPEI and GO were connected with hydrogen bonds.

2.2.2 Preparation of a GO and MMT composite (GO/MMT), and an HPEI-G and MMT composite (HPEI-G/MMT). Firstly, 100 mL solution of 0.5 wt% GO, and 100 mL solution of 0.5 wt% HPEI-G solution were prepared. Next, the GO solution and HPEI-G solution were each mixed with 3 g of MMTto from the GO/MMT dispersion and HPEI-G/MMT dispersion, respectively, and stirred at 80 °C for 16 h. The dispersions were centrifuged at 4000 rpm for 1 h, followed by removal of their supernatants, and washing of the pellets with deionised water. Finally, the pellets were dried at 90 °C for 3 h, followed by grinding into powder.

2.2.3 Preparation of hybrid. Firstly, six portions, each of 10 mL of deionised water were mixed with 0.3 g of MMT, followed by stirring for 16 h. Next, different inhibitors were added to five of the dispersions to obtain different hybrids, in which the concentrations of HPEI-G were 0.1 wt%, 0.3 wt%, 0.5 wt% and 0.7 wt%, and the concentration of GO was 0.5 wt%, followed by stirring for 12 h. The partial hybrids were dried at 90 °C for 4 h, followed by grinding into powder.

2.3 Characterization

2.3.1 Fourier transform infrared spectroscopy (FT-IR). The FT-IR spectra of MMT, GO/MMT and HPEI-G/MMT were recorded on a Spectrum 100 FT-IR spectrometer (PerkinElmer, USA), over the range of 4000 and 400 cm^{-1}.

2.3.2 X-ray diffraction (XRD). The XRD patterns of GO/MMT and HPEI-G/MMT were recorded on a D8 Advance diffractometer (Bruker, Germany), with 2θ angle between 5° and 20°. The interlaminar spacing $d_{(001)}$ was determined using Bragg's equation: $n\lambda = 2d \sin 2\theta$ (where $n = 1$, $\lambda = 0.15406$ nm).

2.3.3 Particle size distribution test. Six hybrids were diluted 100 times, to give a concentration of MMT of 0.03 wt%. Then, the supernatant of the hybrids was removed for testing. The particle size distribution of the hybrids was measured with

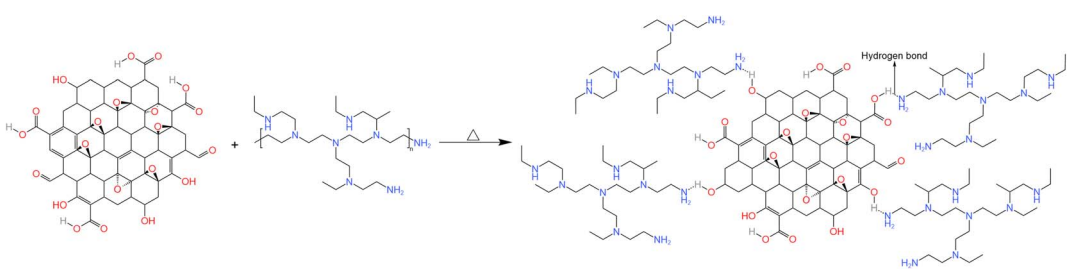

Fig. 1 Preparation process for HPEI-G.

a Zetasizer Nano ZS90 instrument (Malvern Instruments, UK). The testing was performed at 25 °C.

2.3.4 Scanning electron microscopy (SEM). The powder of six hybrids was adhered to sticky tape, followed by metal spraying for 3 min. The SEM images of the powders were measured with a JSE-IT300 instrument (Japan Electronics, Japan). The testing was performed at 25 °C.

2.4 Inhibition evaluation

2.4.1 Mud making test. It is the inhibition of bentonite slurry formation and the maintenance of the drilling fluid rheological properties that are among the most basic requirements for shale inhibitors.[25] Firstly, 17.5 g of MMT was poured into 350 mL water and inhibitor solutions, in which the concentrations of HPEI-G were 0.1 wt%, 0.3 wt% and 0.5 wt%, the concentration of GO was 0.5 wt%, and the concentrations of HPEI and KCI were 1 wt%. Next, the dispersions were stirred at 8000 rpm for 20 min to disperse evenly. The apparent viscosity (AV), plastic viscosity (PV) and yield point (YP) were measured with a ZNN-D6 rotary viscometer (Qingdao Shande Petroleum Instrument Company, China). Next, 17.5 g of MMT was poured into the dispersion again, and the AV, PV and YP of the dispersion were tested after stirring under the same conditions as previously. The process was repeated until the dispersion could not be tested further.[26] Next, the same ratio of dispersion was prepared, and it was then placed in a XGRL-4A high-temperature roller furnace (Qingdao Haitongda Special Instrument Company, China) at a specific temperature (120 °C and 150 °C) for 16 h. The AV, PV and YP of the dispersion were determined after cooling. Next, 17.5 g of MMT was poured into the dispersion again and the AV, PV and YP of the dispersion were determined after measuring under the same conditions. The process was repeated until the dispersion could not be tested further.[26] The AV, PV and YP of the dispersion were calculated according to the following formulas:

$$\mathrm{AV} = 0.5\Phi_{600}\ (\mathrm{mPa\ s}) \quad (1)$$

$$\mathrm{PV} = \Phi_{600} - \Phi_{300}\ (\mathrm{mPa\ s}) \quad (2)$$

$$\mathrm{YP} = \Phi_{300} - 0.5\Phi_{600}\ (\mathrm{Pa}) \quad (3)$$

Φ_{300} is the viscometer reading at 300 rpm, and Φ_{600} is the viscometer reading at 600 rpm.

2.4.2 Linear swelling test. Firstly, 10 g of MMT was poured into a pressure tank, followed by pressure at 10 MPa for 15 min to obtain a lump of soil. Deionised water and inhibitor solutions were prepared (30 mL of each), in which the concentrations of HPEI-G were 0.1 wt%, 0.3 wt%, 0.5 wt% and 0.7 wt%, and the concentration of GO was 0.5 wt%, and the concentrations of HPEI and KCI were 1 wt%. After the linear swell meter (NP-01, Beijing Institute of Exploration Engineering, China) was cleaned, the soil block was placed in it. The test was started and the sample was injected with deionised water and the solutions of different inhibitors to determine the linear swelling rate of MMT over 16 h.

2.4.3 Sedimentation test. The inhibition capability of the inhibitors on the hydration of MMT were determined using sedimentation test.[27] A portion of MMT (3 g) was poured into 100 mL of water and inhibitor solutions, in which the concentrations of HPEI-G were 0.1 wt%, 0.3 wt%, 0.5 wt% and 0.7 wt%, the concentration of GO was 0.5 wt%, and the concentration of HPEI was 1 wt%. Then, the dispersions were stirred for 30 min, followed by pouring into 100 mL graduated cylinders, and the sedimentation height of the MMT was recorded over 3 h.

2.5 Compatibility tests

The slurry was prepared by mixing 350 mL of water with 14 g of MMT and 0.875 g of Na_2CO_3, followed by stirring at 8000 rpm for 20 min and then standing for 16 h. The basic water-based drilling mud (WBM) was prepared with the slurry, in which the concentrations of CMC-LV, XC, PAM, and barite were 0.1, 0.2, 0.5, and 0.5 w/v%, respectively. The WBM with different inhibitors were prepared with the basic WBM, in which the concentrations of HPEI-G and GO were 0.5 wt%, and the concentrations of HPEI and KCl were 1 wt%. The viscosity of WBDF was measured, including AV, PV, YP and gel strength, where the gel strength was obtained from the viscometer readings at 3 rpm after 10 s and 10 min. The filtration volume at 690 kPa after 30 min (FL_{API}) of WBM was recorded with a model SD6A medium-pressure filtration apparatus (Qingdao Haitongda Special Instrument Company, China). After ageing at 150 °C for 16 h, the viscosity and FL_{API} of WBM were determined again.

3. Results and discussion

3.1 Characterisation

The FT-IR spectra of GO/MMT and HPEI-G/MMT were surveyed to investigate the structural characteristics, and they are shown in Fig. 2. Typical characteristics of hydroxyl groups can be observed in the spectrum of GO/MMT. The tensile vibration peak of O–H was at 3468 cm^{-1}, which was wide and blunt.[28] Typical characteristics of amino groups were observed in the

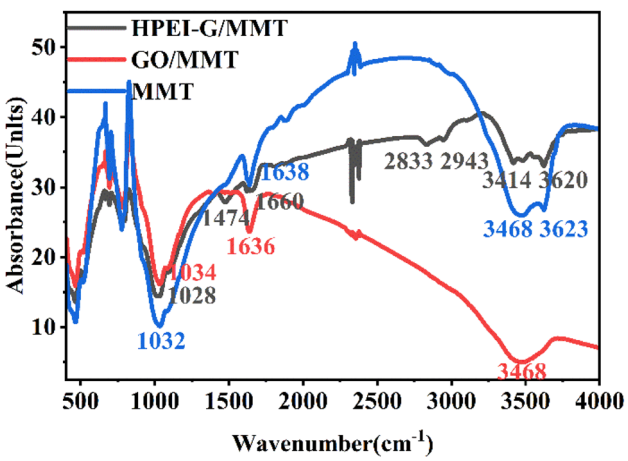

Fig. 2 The FT-IR spectra of MMT, GO/MMT and HPEI-G/MMT.

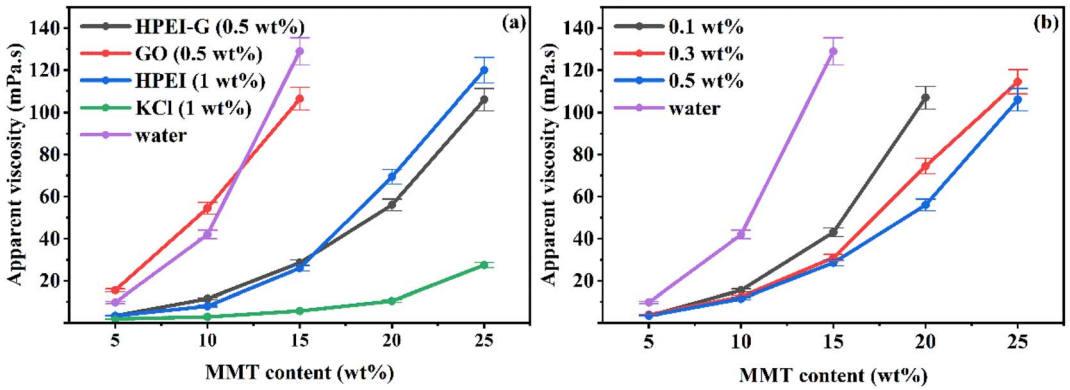

Fig. 3 Apparent viscosity of MMT dispersions changes with the concentrations of MMT at room temperature, (a) with different inhibitors, and (b) with different concentrations of HPEI-G.

spectrum of HPEI-G/MMT. The peaks of N–H at 2833 cm^{-1} and 2934 cm^{-1}, indicating that the HPEI was connected to GO. The tensile vibration peak of O–H in the spectrum of HPEI-G/MMT was 3620 cm^{-1}. Compared with the peak of Si–O in MMT at 1032 cm^{-1}, the peak of Si–O in HPEI-G/MMT was redshifted by 4 cm^{-1}. Compared with the peak of water deformation band in MMT at 1638 cm^{-1}, the peak of water deformation band in HPEI-G/MMT was blueshifted by 22 cm^{-1}, which indicated that the HPEI-G had combined with water in the MMT.

3.2 Inhibition evaluation

3.2.1 Mud making tests. When MMT is dispersed in water, it will significantly increase the flow resistance of the fluid, and the addition of inhibitors can inhibit the hydration of MMT effectively. The lower the viscosity of the fluid, the lower the degree of hydration of MMT, which means the inhibition performance is better. As shown in Fig. 3(a), as the content of MMT increased, the AV also increased. When the content of MMT was 15 wt%, the AV of the MMT dispersion without inhibitor increased sharply, and the AV of the MMT dispersions with inhibitors were lower, all representing different degrees of inhibition. When the content of MMT was 20 wt%, the dispersion containing only water was so viscous that its AV could not be determined, and the addition of partial inhibitors mitigated the increase rate of AV effectively. When the MMT content was 25 wt%, the inhibition capability of HPEI-G was better than the inhibition capability of other inhibitors except for KCl. Table 1 shows that the PV and YP of the MMT dispersion with HPEI-G were lower than those of other inhibitors except for KCl at room temperature. As shown in Fig. 3(b), the dispersion containing 0.5 wt% HPEI-G had the best inhibition ability, and the inhibition effect of HPEI-G increased as the concentration increased. The experimental results showed that HPEI-G had a better inhibition effect than GO without compounding, which meant that HPEI-G significantly reduced the amount of the graphene material required in order to inhibit hydration.

Table 1 Changes of plastic viscosity and yield point of MMT dispersions with different concentrations of MMT at room temperature

	HPEI-G		GO		HPEI		KCl		Water	
MMT (wt%)	PV	YP	PV	YP	PV	YP	PV	YP	PV	YP
5	3.0	1.0	7.0	8.5	3.0	0.5	1.0	0.0	5.0	4.8
10	9.0	3.5	6.5	47.5	5.5	2.5	2.0	1.0	5.0	37.0
15	13.0	18.0	5.0	101.5	9.0	17.0	3.5	2.0	8.5	120.5
20	17.5	57.0			24.0	45.5	5.0	5.5		
25	15.0	99.5					5.0	22.5		

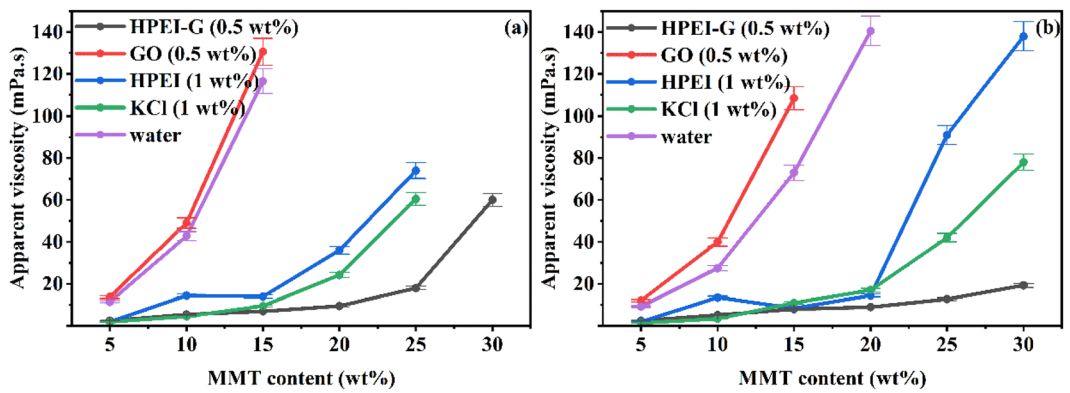

Fig. 4 Apparent viscosity of MMT dispersions changes with the concentrations of MMT after aging at (a) 120 °C, and at (b) 150 °C.

Table 2 Changes of plastic viscosity and yield point of MMT dispersions with different concentrations of MMT after aging at 120 °C

	HPEI-G		GO		HPEI		KCl		Water	
MMT (%)	PV	YP	PV	YP	PV	YP	PV	YP	PV	YP
5	2.0	0.5	6.5	7.3	2.0	0.0	1.5	0.5	6.0	5.5
10	5.5	0.0	11.0	38.0	5.5	9.0	3.0	1.5	12.5	30.3
15	7.0	0.0	11.5	119.0	9.5	4.5	4.0	5.5	13.0	103.5
20	9.0	0.5			18.0	18.0	7.0	17.5		
25	16.0	2.0			22.0	52.0	4.0	56.5		
30	31.0	29.0								

Table 3 Changes of plastic viscosity and yield point of MMT dispersion with different concentrations of MMT after aging at 150 °C

	HPEI-G		GO		HPEI		KCl		Water	
MMT (%)	PV	YP	PV	YP	PV	YP	PV	YP	PV	YP
5	2.0	0.5	6.0	6.0	2.0	0.0	1.0	0.5	5.5	3.8
10	5.5	0.0	10.5	29.5	7.0	6.5	2.5	1.0	10.0	17.5
15	7.5	0.5	29.0	79.5	7.0	1.5	4.0	7.0	15.0	58.0
20	9.0	0.0			11.0	3.5	5.5	11.5	16.0	124.5
25	12.5	0.5			34.5	56.5	6.5	35.5		
30	15.5	4.0			31.5	106.5	3.0	75.0		
35	30.0	19.0					5.0	142.0		

Fig. 4(a) shows that after ageing at 120 °C, when the content of MMT was 15 wt%, the dispersion containing only water was so viscous that its AV could not be determined, and the addition of partial inhibitors mitigated the increase rate of AV effectively. When the content of MMT was 30 wt%, the others were too viscous to measure its AV except for the dispersion with HPEI-G. Fig. 4(b) shows that after ageing at 150 °C, when the content of MMT was 20 wt%, the dispersion containing only water was so viscous that its AV could not be determined. The inhibition effect of HPEI-G was strikingly lower than that of the other inhibitors. And when the content of MMT was 30 wt%, the AV of the dispersion with HPEI-G can be maintained below 20 mPa s. As shown in Fig. 4, after ageing at 120 °C and 150 °C, the order of inhibition capacity of the inhibitors was HPEI-G > KCl > HPEI > GO. As shown in Tables 2 and 3, after ageing at 120 °C and 150 °C, the PV of the MMT solution with HPEI-G was lower than that of other inhibitors except for KCl, and the YP of the MMT solution with HPEI-G was the lowest. The experimental results showed that HPEI-G had a better inhibition effect at high temperature than at room temperature.

3.2.2 Linear swelling tests. The capacity of inhibitors to inhibit MMT hydration is shown by the linear swelling tests. Fig. 5(a) shows the linear swelling rate with various inhibitors over 16 h. It was observed that the MMT swelled rapidly in deionised water without inhibitors, and its swelling rate was 64.49%. Thus, the inhibitors were effective at alleviating the hydration of MMT. The traditional inhibitor KCl decreased the swelling rate of MMT to 43.83%, and the inhibition effects of GO and HPEI were similar to that of KCl. The HPEI-G reduced the swelling rate of MMT to 30.36%, which significantly alleviated the hydration of MMT, and the concentration of HPEI-G tested was only half of the concentration required using KCl. Fig. 5(b) shows the linear swelling rate with HPEI-G at different concentrations. It was observed that when 0.1 wt% HPEI-G was used, the swelling rate of MMT was strikingly decreased, and as the concentration increased, the inhibition performance of the HPEI-G also increased. The expansion curve of MMT in HPEI-G solution had a similar shape to that in KCl solution, which indicated that HPEI-G may have an inhibition mechanism in common with KCl.

3.2.3 Sedimentation tests. Fig. 6(a) shows the sedimentation height of MMT in different inhibitor solutions and deionised water. It was observed that the sedimentation height in GO solution was similar to that in deionised water, which meant that the inhibition capability of GO was not good. Whereas in HPEI and HPEI-G solutions, the sedimentation height decreased rapidly, which meant that the inhibition performances of HPEI and HPEI-G were excellent. The concentration of HPEI-G was only half of the concentration of HPEI, which indicated that after the combination of HPEI and GO, the inhibition performance of the composite was improved. Fig. 6(b) shows the sedimentation height of MMT in HPEI-G solutions of different concentrations. It was observed that at a low concentration, the inhibition effect of HPEI-G increased as its concentration increased. After the concentration of

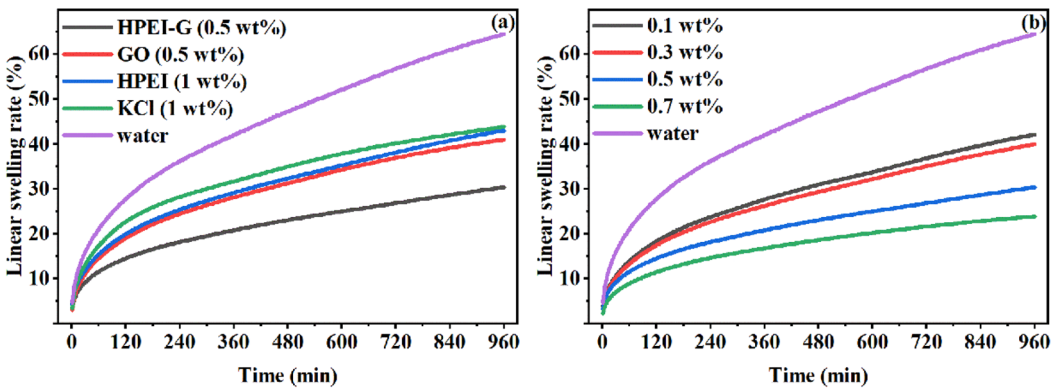

Fig. 5 Linear swelling rate of MMT at room temperature with (a) different inhibitors, and (b) different concentrations of HPEI-G.

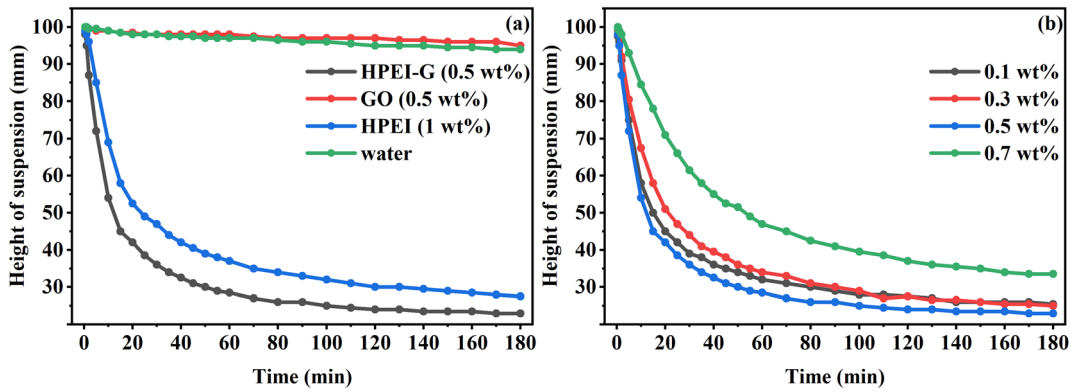

Fig. 6 The sedimentation height of the MMT suspension at room temperature with (a) different inhibitors, and (b) different concentrations of HPEI-G.

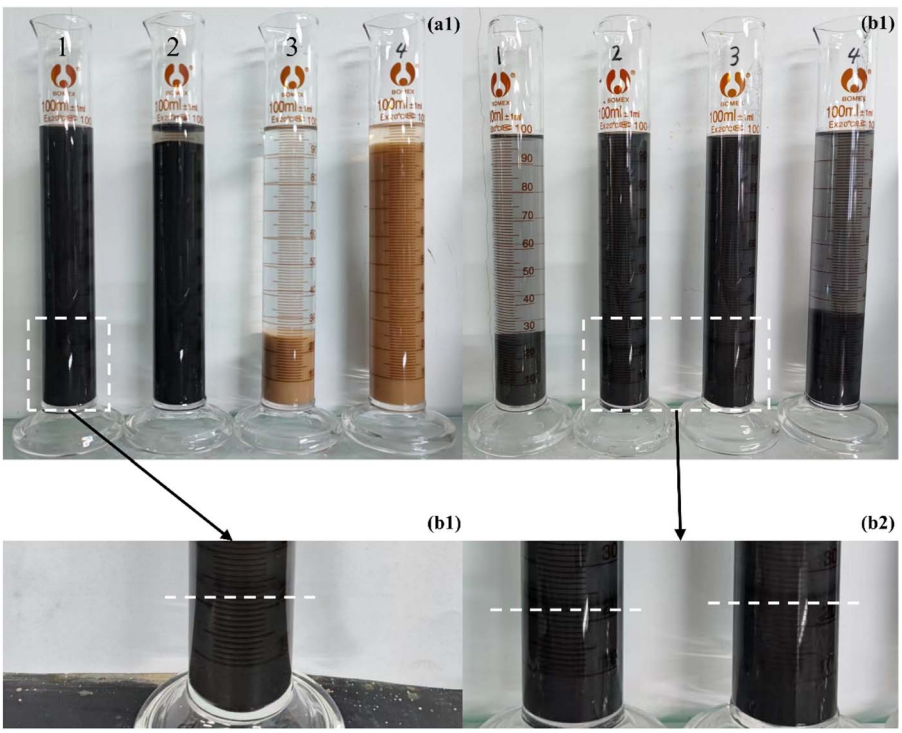

Fig. 7 Sedimentation behaviour of MMT at room temperature, (a) different inhibitors, from 1 to 4: HPEI-G, GO, HPEI and water, and (b) different concentrations of HPEI-G, from 1 to 4: 0.1 wt%, 0.3 wt%, 0.5 wt% and 0.7 wt%.

0.5 wt%, the inhibition effect of HPEI-G decreased as the concentration increased. Compared with GO, HPEI-G consisted of a hyperbranched polymer with graphene material, which highlighted the improvement of the structural stability of hyperbranched polymers on clay mineral particles.

Fig. 7 shows the sedimentation behaviour of MMT at room temperature. The experimental results indicated that the inhibition effect was best when the HPEI-G concentration was 0.5 wt%. This may be due to the fact that when the concentration was above 0.5 wt%, the dehydration ability for the hydrated MMT particles reduced as the degree of polymerisation of HPEI-G in water increased.

3.3 Inhibition mechanism

3.3.1 The XRD analysis. Fig. 8 shows the XRD patterns of HPEI-G/MMT, GO/MMT and MMT. The interlaminar spaces of MMT, GO/MMT and HPEI-G/MMT were 12.01, 12.07 and 13.63 Å, respectively, which meant the interlaminar space of HPEI-G with MMT increased to 1.62 Å. Because the hydrogen bond length was about 2 Å, it was believed that the hydrogen bond was formed between HPEI-G and MMT through the HPEI molecule. The results showed HPEI-G can be adsorbed on the clay mineral surfaces and between the layers.

3.3.2 Particle size distribution analysis. After full hydration, the particles of MMT were mainly fine particles. The diffuse

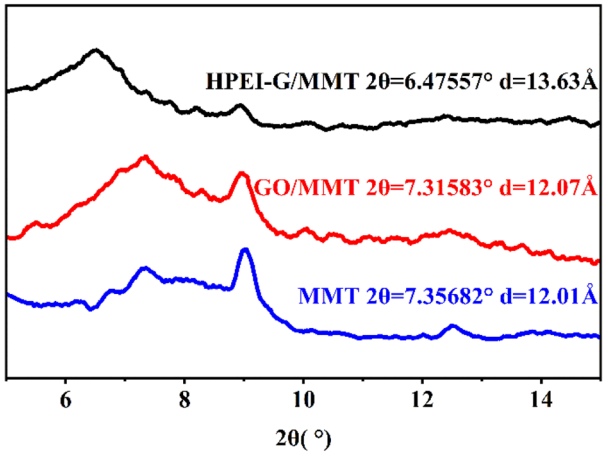

Fig. 8 The XRD patterns of HPEI-G/MMT, GO/MMT and MMT.

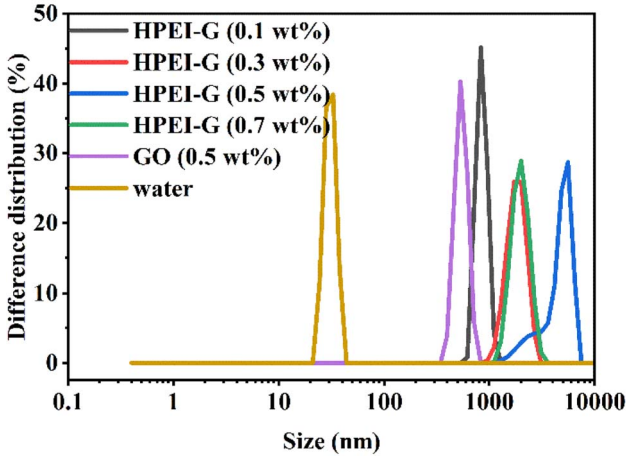

Fig. 9 Difference particle size distribution of MMT particles.

double layer was compressed so that the particles of MMT accumulated, resulting in an increase in particle size. Therefore, the inhibition effect of the inhibitor was positively correlated with the particle size of MMT. As shown in Fig. 9, the particle size of MMT in inhibitor solutions increased, and the increase in the particle size in HPEI-G solution was higher than that of GO with the same concentration. The particles of the hybrid with GO were larger than those of hybrid without inhibitors, because the graphene sheets were attached to the clay particles, but GO cannot inhibit clay hydration more efficiently because it had a low dewatering capacity against hydrated clay particles. It was also observed that the inhibition effect of HPEI-G increased as the concentration increased at low concentrations. When the concentration was greater than 0.5 wt%, the inhibition effect of HPEI-G decreased as the concentration increased. When the concentration was 0.5 wt%, HPEI-G had the strongest dehydration capacity for hydrated MMT particles, and this explained the results of the sedimentation test.

3.3.3 The SEM analysis. Porosity is positively correlated with water entering the pores and the hydration of clay particles. Fig. 10 shows the SEM image of the hybrid combined with the fully hydrated MMT, and different inhibitors. It was observed from Fig. 10(c) and (f) that the surface of the MMT hybrid without inhibitor was uneven, and the surface of MMT hybrid compounded with 0.5 wt% HPEI-G was dense, and the pores were small. This indicated that after compounding with the inhibitor, the aggregation of clay particles was stronger due to the adsorption between the clay and the inhibitors. From Fig. 10(a), (b), (d) and (e), it was observed that the microscopic morphology of the MMT hybrids compounded with 0.1 wt% HPEI-G, 0.3 wt% HPEI-G, 0.7 wt% HPEI-G and 0.5 wt% GO were uneven, containing pores and particles, which were consistent with the results of the particle size distribution test. It was observed that the pores of the MMT hybrid without inhibitor were larger, whereas the surfaces of the MMT hybrids

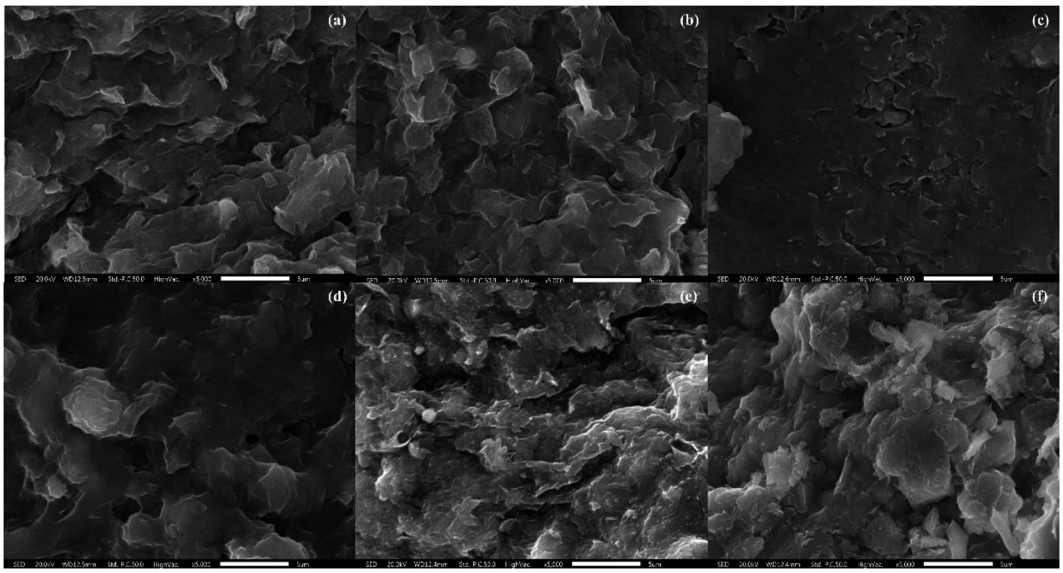

Fig. 10 The SEM image of the hybrid combined with the fully hydrated MMT and (a) 0.1 wt% HPEI-G, (b) 0.3 wt% HPEI-G, (c) 0.5 wt% HPEI-G, (d) 0.7 wt% HPEI-G, (e) 0.5 wt% GO, and (f) water.

Table 4 The viscosity and FL_{API} of WBM

Ageing	AV (mPa s)	PV (mPa s)	YP (Pa)	Gel strength (10 s/10 min)	FL_{API} (mL)
Before	29.5	15.0	14.5	12.0/15.0	7.0
After	30.5	17.0	13.5	8.0/12.0	6.6

Table 5 The ratio of the viscosity and FL_{API} of WBM with different inhibitors to WBM without inhibitor

Ageing	Dispersion	AV	PV	YP	FL_{API}
Before	WBDF + 0.5 wt% HPEI-G	1.085	1.467	0.690	1.114
	WBDF + 0.5 wt% GO	0.729	0.933	0.483	1.200
	WBDF + 1 wt% HPEI-G	1.169	1.467	0.828	0.886
	WBDF + 1 wt% KCl	0.712	0.867	0.552	1.029
After	WBDF + 0.5 wt% HPEI-G	0.869	1.000	0.704	1.061
	WBDF + 0.5 wt% GO	0.689	0.706	0.667	1.061
	WBDF + 1 wt% HPEI-G	0.803	0.941	0.630	1.364
	WBDF + 1 wt% KCl	0.803	0.647	1.000	1.576

compounded with 0.3 wt% HPEI-G and 0.7 wt% HPEI-G had smaller pores, and the surface of the MMT hybrids compounded with 0.5 wt% HPEI-G were not observed to have pores, which indicated that the smaller the porosity, the better its ability to inhibit hydration.

3.3.4 Probable inhibition mechanism. The inhibition mechanism of HPEI-G included chemical adsorption and physical blockage. When the HPEI-G was dispersed in water, the amino groups on the HPEI molecule formed cations that bound to anions on the surface of the MMT. HPEI-G was adsorbed on the surface and interlayer of MMT by hydrogen bonding and electrostatic attraction, reducing the diffuse electric double layer to inhibit the hydration of MMT. Furthermore, the sheets of graphene in HPEI-G allowed it to attach to nanopores and microcracks, clogging the nanopores and blocking water from passing through the nanopores, thereby inhibiting the hydration of the clay minerals. When the concentration of HPEI-G was higher than 0.5 wt%, the ability to prevent water from entering the clay surface increased as the degree of polymerisation of HPEI-G in water increased, but the dehydration ability for the hydrated MMT particles reduced.

3.4 Compatibility tests

The difference in the viscosity and FL_{API} of WBM before and after the addition of the inhibitor showed the compatibility of the inhibitor with WBM. Table 4 shows the viscosity and FL_{API} of WBM before and after ageing. Table 5 shows the ratio of the viscosity and FL_{API} of WBM, with and without inhibitor. It was observed that before and after ageing, HPEI-G had little impact on the reliability of WBM. Therefore, it was considered that HPEI-G has good compatibility with the ordinary drilling fluid additives.

4. Conclusions

In this work, we prepared HPEI-G, a composite based on HPEI and GO, and used it as a shale inhibitor to test its inhibition performance, determine its inhibition mechanism, and evaluate its compatibility in WBM. It was observed from the linear swelling test that 0.5 wt% HPEI-G reduced the swelling rate of MMT to 30.36%, and KCl only decreased the swelling rate of MMT to 43.83%, the concentration of which was double that of HPEI-G. The inhibition performance evaluation tests proved that the inhibition effect of HPEI-G was better than that of other inhibitors, and the addition of HPEI-G was less. From the SEM, it was observed that the surface of MMT hybrid compounded with 0.5 wt% HPEI-G was dense and the pores were small. The inhibition mechanism of HPEI-G included chemical adsorption and physical blockage. HPEI-G was adsorbed on the surface and interlayer of MMT by hydrogen bonding and electrostatic attraction, thus reducing the diffuse electric double layer to inhibit the hydration of MMT. The sheets of graphene in HPEI-G allowed it to stick on the surface of shale and it plug the nanopores of shale, preventing the access of water. The inhibition effect of HPEI-G in WBDF over a temperature range from room temperature to 150 °C was considered to be excellent.

Conflicts of interest

There are no conflicts to declare.

Acknowledgements

We would like to thank the Basic Research Program on Deep Petroleum Resource Accumulation and Key Engineering Technologies (U19B6003) for their financial support of this work.

References

1 J. Zhang, *Int. J. Rock Mech. Min. Sci.*, 2013, **60**, 160–170.
2 N. S. Muhammed, T. Olayiwola and S. Elkatatny, *J. Pet. Sci. Eng.*, 2021, **206**, 109043.
3 A. Rana, M. K. Arfaj and T. A. Saleh, *Fuel*, 2019, **247**, 237–249.
4 M. K. Al. Arfaj, M. Amanullah, S. Aramco, A. S. Sultan, E. Hossain and A. Abdulraheem, *Chemical and Mechanical Aspects of Wellbore Stability in Shale Formations: A Literature Review*, Society of Petroleum Engineers, 2014.
5 T. Ma and P. Chen, *J. Nat. Gas Sci. Eng.*, 2015, **26**, 72–98.
6 R. Gholami, H. Elochukwu, N. Fakhari and M. Sarmadivaleh, *Earth-Sci. Rev.*, 2018, **177**, 2–13.
7 J. Hermoso, F. Martinez-Boza and C. Gallegos, *Appl. Clay Sci.*, 2014, **87**, 14–21.
8 G. Zhuang, Z. Zhang, M. Fu, X. Ye and L. Liao, *Appl. Clay Sci.*, 2015, **116–117**, 257–262.
9 X. Li, G. Jiang, L. Yang, K. Wang, H. Shi, G. Li and X. Wu, *Energy Fuels*, 2019, **33**, 9342–9350.
10 G. Xie, P. Luo and M. Deng, *Chem. Technol. Fuels Oils*, 2016, **52**, 542–549.
11 R. de C. Balaban, E. L. F. Vidal and M. R. Borges, *Appl. Clay Sci.*, 2015, **105–106**, 124–130.
12 Y. An, G. Jiang, Y. Ren, L. Zhang, Y. Qi and Q. Ge, *J. Pet. Sci. Eng.*, 2015, **135**, 253–260.
13 J. G. Xu, Z. Qiu, X. Zhao, Y. Zhang, G. Li and W. Huang, *J. Surfactants Deterg.*, 2018, **21**, 155–164.

14 Y. Liu, L. Chen, Y. Tang, X. Zhang and Z. Qiu, *Rev. Adv. Mater. Sci.*, 2022, **61**, 186–194.
15 Y. Liu, Y. Tang, Q. Chang, C. Ma, S. He and L. Yuan, *Nanotechnol. Rev.*, 2022, **11**, 2786–2799.
16 P. Mathumba, A. T. Kuvarega, L. N. Dlamini and S. P. Malinga, *Mater. Lett.*, 2017, **195**, 172–177.
17 J. Guancheng, Q. Yourong, A. Yuxiu, H. Xianbin and R. Yanjun, *Appl. Clay Sci.*, 2016, **127–128**, 70–77.
18 D. v. Kosynkin, G. Ceriotti, K. C. Wilson, J. R. Lomeda, J. T. Scorsone, A. D. Patel, J. E. Friedheim and J. M. Tour, *ACS Appl. Mater. Interfaces*, 2012, **4**, 222–227.
19 A. Yuxiu, J. Guancheng, Q. Yourong, H. Xianbin and S. He, *J. Nat. Gas Sci. Eng.*, 2016, **32**, 347–355.
20 A. Rana and T. A. Saleh, *Improvement in Rheological Features, Fluid Loss and Swelling Inhibition of Water-Based Drilling Mud by Using Surfactant-Modified Graphene*, Society of Petroleum Engineers, 2019.
21 T. A. Saleh and M. A. Ibrahim, *Energy Rep.*, 2019, **5**, 1293–1304.
22 T. A. Saleh, A. Rana and M. K. Arfaj, *Environ. Nanotechnol. Monit. Manag.*, 2020, **14**, 100348.
23 A. Rana, M. K. Arfaj and T. A. Saleh, *Appl. Clay Sci.*, 2020, **199**, 105806.
24 A. Rana, M. K. Arfaj, A. S. Yami and T. A. Saleh, *J. Environ. Chem. Eng.*, 2020, **8**, 103802.
25 Q. Chu, L. Lin and Y. Zhao, *J. Pet. Sci. Eng.*, 2019, **182**, 106333.
26 F. T. G. Dias, R. R. Souza and E. F. Lucas, *Fuel*, 2015, **140**, 711–716.
27 J. Ma, S. Pang, W. Zhou, B. Xia and Y. An, *Energy Fuels*, 2021, **35**, 7833–7843.
28 C. I. R. de Oliveira, M. C. G. Rocha, A. L. N. da Silva and L. C. Bertolino, *Ceramica*, 2016, **62**, 272–277.